Earthquakes and Structures, *Vol. 16, No. 2 (2019) 235-251*
DOI: https://doi.org/10.12989/eas.2019.16.2.235

Investigations on the behaviour of corrosion damaged gravity load designed beam-column sub-assemblages under reverse cyclic loading

A. Kanchanadevi*[1,2] and K. Ramanjaneyulu[1,2a]

[1]*CSIR-Structural Engineering Research Centre, Chennai, Tamil Nadu, India*
[2]*Academy of Scientific and Innovative Research (AcSIR), India*

(Received November 14, 2018, Revised December 31, 2018, Accepted January 22, 2019)

Abstract. Corrosion of reinforcement is the greatest threat to the safety of existing reinforced concrete (RC) structures. Most of the olden structures are gravity load designed (GLD) and are seismically deficient. In present study, investigations are carried out on corrosion damaged GLD beam-column sub-assemblages under reverse cyclic loading, in order to evaluate their seismic performance. Five GLD beam-column sub-assemblage specimens comprising of i) One uncorroded ii) Two corroded iii) One uncorroded strengthened with steel bracket and haunch iv) One corroded strengthened with steel bracket and haunch, are tested under reverse cyclic loading. The performances of these specimens are assessed in terms of hysteretic behaviour, energy dissipation and strength degradation. It is noted that the nature of corrosion i.e. uniform or pitting corrosion and its location have significant influence on the behaviour of corrosion damaged GLD beam-column sub-assemblages. The corroded specimens with localised corrosion pits showed in-cyclic strength degradation. The study also reveals that external strengthening which provides an alternate force path but depends on the strength of the existing reinforcement bars, is able to mitigate the seismic risk of corroded GLD beam-column sub-assemblages to the level of control uncorroded GLD specimen.

Keywords: corrosion; beam-column sub-assemblage; gravity load designed; energy dissipation; hysteretic behaviour; reverse cyclic loading; in-cyclic strength degradation

1. Introduction

Most of the olden reinforced concrete (RC) structures might have undergone environmental degradation due to corrosion of reinforcement steel. In a tropical country like India which has very long coast line, temperature and humidity conditions are conducive for corrosion of reinforcement steel. From the corrosion map of India, it could be witnessed that the extreme and severe rate of corrosion is found to be 0.2 and 0.1-0.2 mm per year respectively (Natesan *et al*. 2005). Further, these olden structures were gravity load designed (GLD), i.e., designed to carry self-weight and imposed loads, and detailed accordingly. Hence, these RC structures are deficient to cater for seismic loading and also exhibited poor performance in the past earthquakes such as Killari (Jain *et al*. 1994), Bhuj (Humar *et al*. 2001) etc. This signifies the need for understanding the seismic performance of existing corrosion affected GLD RC structures.

In general, any element or compound remains stable when its free energy is minimised. Iron oxide is the thermodynamically stable form of iron and exists in that form. Hence, steel oxidises to iron oxides (rust) spontaneously. Thus, corrosion of reinforcement is unavoidable because it is a spontaneous process. Corrosion of steel in reinforced concrete is an electrochemical process involving anodic and cathodic reactions in the presence of water and oxygen as shown in Fig. 1.

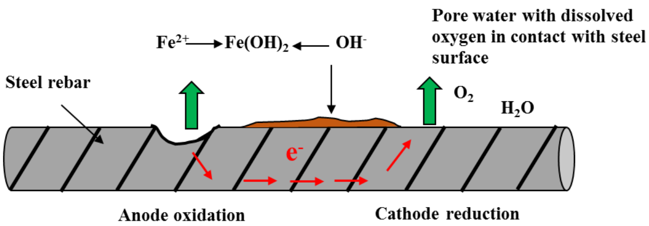

Fig. 1 Corrosion of reinforcement steel in concrete

At active corrosion sites, iron atom of rebar loses its valence electrons and form ferrous ion. The liberated electrons from the oxidation of iron flow to the cathodic sites where the electrons are consumed by oxygen and water present in the concrete and form hydroxyl ion (OH^-). The ferrous ions react with hydroxyl ions and form ferrous hydroxide. Ferrous hydroxide ($Fe(OH)_2$) undergoes further reactions to form different forms of ferrous hydroxides and oxides. Thus, as soon as the corrosion is induced, the iron forms its corresponding oxide whose volume is two to three times the original volume of the reinforcement. The volume of rust produced plays a significant role in subsequent damage induced to the structure. The corrosion of reinforcement causes reduction in the mechanical properties of reinforcement and also results in the substantial reduction in the elongation of reinforcement which is a vital material

*Corresponding author, Ph.D. Student
E-mail: kanchana@serc.res.in
[a]Ph.D.
E-mail: rams@serc.res.in

characteristic from seismic view point (Zhu and Francois 2013, Imperatore *et al*. 2017). The bond degradation of corroded members was studied and models were proposed to evaluate the reduction in bond strength due to corrosion by Lee *et al*. (2002), Fang *et al*. (2006), Bhargava *et al*. (2007), Chung *et al*. (2008), Wang (2009), Wu *et al*. (2016), Zhou *et al*. (2017). These models are either statistical or empirical or analytical in nature for the prediction of bond degradation due to corrosion of reinforcement.

Numerous experimental investigations were carried out to evaluate the seismic performance of existing GLD structures with different deficiencies, such as use of smooth mild steel bars, joints lacking stirrups, beam reinforcement with substandard anchorage detailing, lack of confinement in the disturbed region, and inadequate main reinforcement to resist seismic loads (Kunnath *et al*. 1995, El-Attar *et al*. 1997, Calvi *et al*. 2001, Pantelides *et al*. 2002, Dhakal *et al*. 2005, Yavari *et al*. 2013, Melo *et al*. 2015, Kanchanadevi and Ramanjaneyulu 2017). The poor seismic performances of GLD structures were very well documented in the above studies by carrying out experimental investigations on beam-column joint or representative frame or building. Exhaustive studies were carried out on pre-earthquake and post-earthquake retrofit of reinforced concrete deficient beam-column sub-assemblages using epoxy injection, reinforced concrete jacketing, fibre reinforced ultra-high strength concrete jacket or by combining jacketing with other techniques (Tsonos and Papanikolaou 2003, Kakaletsis *et al*. 2011, Tsonos 2014, Kalogeropoulos *et al*. 2016). More recently, numerous efforts were made by researchers to strengthen these seismically deficient structures using external strengthening due to ease of implementation. The external strengthening of the beam-column sub-assemblages was accomplished by providing (i) FRP laminates or FRP sheets around the beam-column joints or combination of FRP and reinforcement (Pampanin *et al*. 2007, Tsonos 2008, Sezen 2012, Realfonzo *et al*. 2014, Hadigheh *et al*. 2014). (ii) by providing steel cages, steel haunch, prestressed steel angles or steel *L* profiles on top and bottom faces of the floor beams (Sharma *et al*. 2014, Campione *et al*. 2015, Santarsiero and Masi 2015, Kheyroddin *et al*. 2016, Kanchanadevi *et al*. 2018). Even though FRP strengthening schemes were successfully employed for seismic strengthening, providing proper anchorage is difficult. The strengthening by addition of steel elements involves either strengthening of the deficient component or providing an alternate force path. The external strengthening by providing an alternate force path is gaining popularity vowing to its ease of implementation.

The seismic performances of corroded structural components, namely beams and columns were evaluated by Li *et al*. (2009), Cardone *et al*. (2013), Goksu and Ilki (2016), Ou and Nguyen (2016). Yuksel (2015) evaluated the dynamic response of typical four storied building frame with corroded reinforcement. The effect of corrosion was incorporated by reduction in area of cross-section, reduction in mechanical properties and reduction in bond strength and modulus of elasticity. It was reported that the strength and ductility were affected and reduced. Liu *et al*. (2017) evaluated seismic performance of corroded RC moment resisting frame under reverse cyclic loading. Impressed current technique was used for inducing reinforcement corrosion. The load drop was nearly linear with increase in corrosion ratio, for the corrosion ratios considered in their study. Guan and Zheng (2018) evaluated the seismic performance of corrosion damaged interior beam column joint due to acid rain. Decrease in load carrying capacity and energy dissipation with the increase in level of corrosion was observed. Kanchanadevi and Ramanjaneyulu (2018b) studied the effect of corrosion on performance of ductile and non-ductile exterior beam-column sub-assemblage designed for seismic loads. It was observed that corrosion of beam reinforcement resulted in reduction in ductility and change in failure mode of beam-column sub-assemblages. Further, the imminent risk associated with corrosion affected beam-column sub-assemblage designed for seismic load was highlighted.

From the reported studies, it could be observed that significant efforts were made to characterize the effects of corrosion at material level and considerable efforts were also made to study the performance of corroded members at component level. Few attempts were made to study the seismic performance of corroded members at sub-assemblage and structural levels. However, the studies on seismic performance of corrosion damaged gravity load designed exterior beam column sub-assemblage were not reported. In reinforced concrete GLD structures, the exterior beam-column joints are the most critical components due to improper force transfer mechanism. Further, the exterior beam-column sub-assemblages are more prone to corrosion due to exposure to aggressive environment. Hence, in present study experimental investigations are carried out on uncorroded and corrosion damaged gravity load designed exterior beam-column sub-assemblages subjected to reverse cyclic loading to evaluate the influence of corrosion on their seismic performance. The seismic performances of the corrosion damaged and uncorroded GLD beam-column sub-assemblages are compared in terms of energy dissipation, load-displacement hysteresis and strength degradation. Further, investigations on corroded beam-column sub-assemblage externally strengthened with steel bracket and haunch scheme are also carried out.

2. Details of the gravity load designed beam-column sub-assemblages

Five full scale gravity load designed beam-column-sub-assemblages with straight bar anchorage at beam bottom are taken up for experimental investigation. The sizes of the beam and column segments and the overall dimensions of the beam-column sub-assemblage are as shown in the Fig. 2(a). The reinforcement details of the specimens are as shown in the Fig. 2(b). The reinforcement cages are prepared according to the detailing presented in Fig. 2(b). The beam top bars are provided with code specified development length whereas the beam bottom bars project straight into the joint as they are meant only to cater for mid span bending moment as per the olden Indian practice.

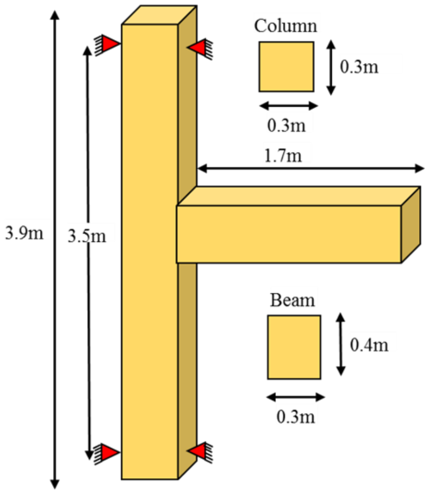

(a) Geometrical details

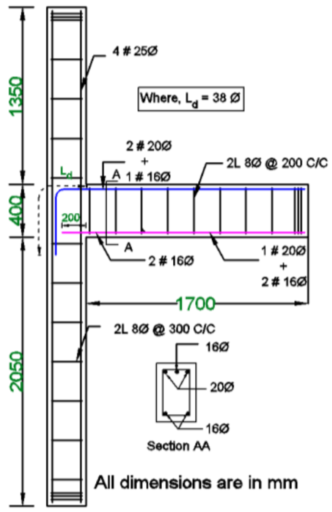

(b) Reinforcement details

Fig. 2 Geometrical and reinforcement details of beam-column sub-assemblage

Further, the joint of the sub-assemblage is not provided with ties as it is typical construction practice of olden times. The concrete mix of 1(cement):1.695(Sand): 3.013(Coarse aggregate) with water/cement ratio of 0.5 is used for casting of the beam-column specimens. The material properties of concrete are evaluated by testing representative cylinder specimens. The beam-column specimens are wet cured for a period of 28 days. After completion of curing period, three of the specimens (designated as SP1-C1, SP1-C2 and SP1-C3-R1) are subjected to accelerated corrosion using impressed current technique. The other two GLD specimens are uncorroded and designated as SP1. The material properties of concrete and reinforcement bars used are presented in Tables 1 and 2 respectively.

3. Accelerated corrosion of GLD beam-column sub-assemblages

In this study, it is aimed to simulate the chloride induced corrosion of reinforcement in concrete structures that are exposed to marine environment. As the process of natural corrosion is very slow, reinforcement bars are subjected to accelerated corrosion by using impressed current technique. The main reinforcement bars at beam top and bottom are proposed to be corroded, for a length equal to twice the depth of the beam along the length of the beam and also the part of rebar projecting into the joint. This defines the region of interest for accelerated corrosion. Typical steps adopted for accelerated corrosion of beam main reinforcement bars of beam-column sub-assemblages are depicted in Fig. 3. The contact surfaces of column main bars, ties and beam stirrups with the main reinforcement bars of beam are insulated as shown in Fig. 3(a). The specimens are cast using steel mould as shown in Fig. 3(b). Brick wall is erected around the region of interest as shown in Fig. 3(c) for creating the pool of electrolyte and to expose the specimen to electrolyte solution. The beam segment adjoining joint region and the joint are immersed in 3.5% NaCl electrolyte solution as shown in Fig. 3(d). In order to induce accelerated corrosion, beam reinforcement bars are connected to the positive terminals of regulated power source and act as anode. The stainless steel plates are connected to the negative terminal of regulated power source and act as cathode as shown in Fig. 3(e). Figs. 3(f) and 3(g) respectively show the view of the specimen during

Table 1 Strength parameters of concrete

Specimen ID	Average cylinder compressive strength (N/mm^2)	Average split tensile strength (N/mm^2)
SP1	41.34	3.7
SP1-C1	47.5	4.27
SP1-C2	41.99	3.78
SP1-C3-R1	41.02	3.79

Table 2 Material properties of steel reinforcement

Diameter of reinforcement bar (mm)	Yield strength of steel (N/mm^2)
8	527
16	545
20	520
25	535

Table 3 Details of accelerated corrosion and level of corrosion of specimens

Specimen ID	Description	Corrosion Current (A)	Duration of corrosion	Average level of corrosion (%) based on gravimetric method	
				Beam top bars	Beam bottom bars
SP1	Control GLD	-	-	-	-
SP1-C1	Corroded GLD	1.29	44 days	6	14
SP1-C2	Corroded GLD	1.57	79 days	10.9	13.8
SP1-C3-R1	Corroded and Strengthened GLD	1.71	79 days	14.2	24
SP1-R1	Strengthened GLD	-	-	-	-

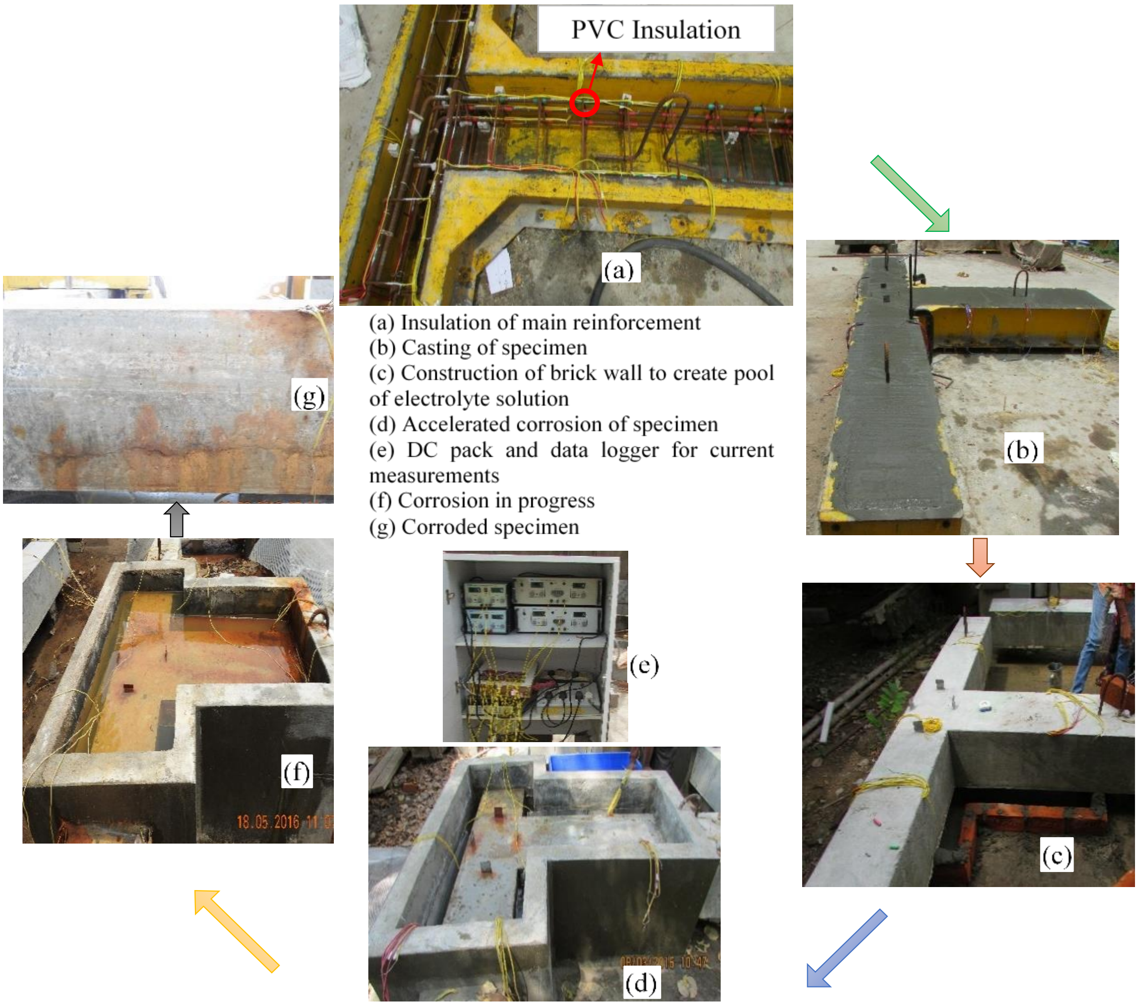

Fig. 3 Typical steps in accelerated corrosion of the beam-column specimens

the accelerated corrosion process and the corrosion stains observed on beam segment. The current in each rod is measured using the data logger till the end of corrosion process and the data is stored. Total average current and duration of current passed in the specimens are presented in Table 3.

4. Steel bracket and haunch strengthening system

For the corroded GLD specimen SP1-C3-R1, external strengthening is carried out using bracket and haunch assembly as shown in Fig. 4, for reducing the shear and moment at joint and preventing anchorage failure of beam bottom reinforcement bars. Further, one of the control uncorroded GLD specimens is also externally strengthened with bracket and haunch system and designated as SP1-R1, which would be a reference specimen for comparison of performance of strengthened corroded GLD specimen SP1-C3-R1. The haunch would act as a prop and thereby reducing forces at the joint face and enabling the development of beam bottom bars. The haunch is connected to the beam at distance of 400 mm from the face of the joint based on the development length requirement of beam bottom bars. The vertical component of haunch force produces shear opposite to beam tip loading and horizontal component of haunch force produces moment opposite to the moment due to beam tip loading. This in turn reduces the beam moment demand at the face of the joint and also joint shear demand. Thus, the introduction of haunch would direct the failure of beam-column sub-assemblage towards the beam by reversing the strength hierarchy. Further, provision of bracket would prevent the opening-up of wider cracks at the face of the joint due to anchorage failure in GLD specimen under upward loading.

5. Experimental investigations on uncorroded and corroded GLD beam-column sub-assemblages

The uncorroded and corroded GLD specimens are instrumented with LVDTs (linear variable displacement transducers), to measure deflections along the length of beam and column segments. The schematic diagram of test set-up for application of reverse cyclic load and positioning of test specimen is shown in Fig. 5. An axial load of 300 kN is applied to the column. Lateral load at the beam tip is applied using 250 kN actuator. The load is applied in displacement control mode according to the loading history shown in Fig. 6 in terms of drift ratio (%). In present study,

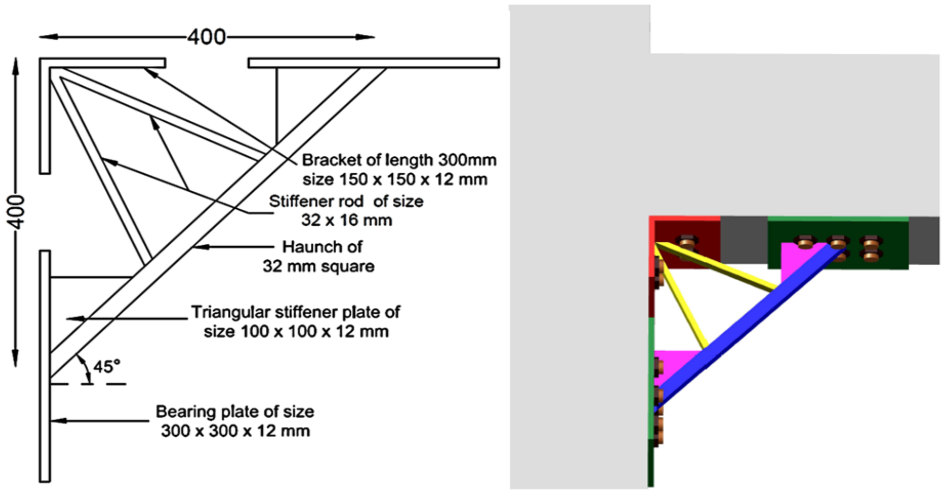

Fig. 4 Geometrical details and schematic view of bracket and haunch strengthening system

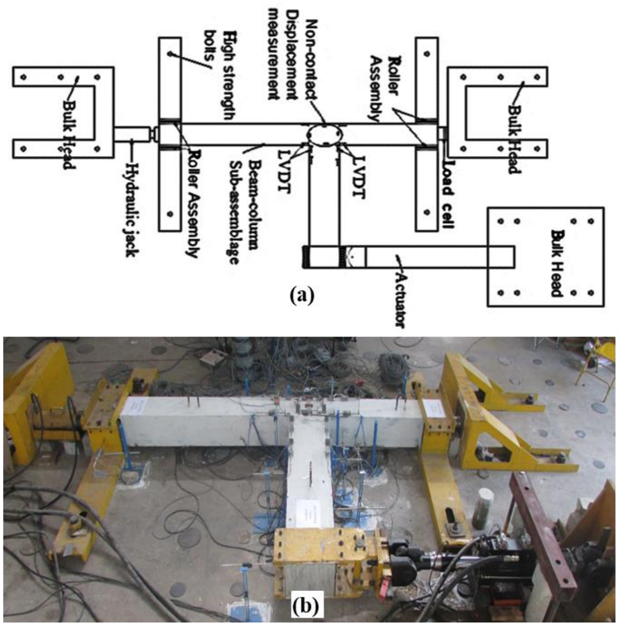

Fig. 5(a) Schematic view of test setup (b) Actual test setup for reverse cyclic loading of specimens

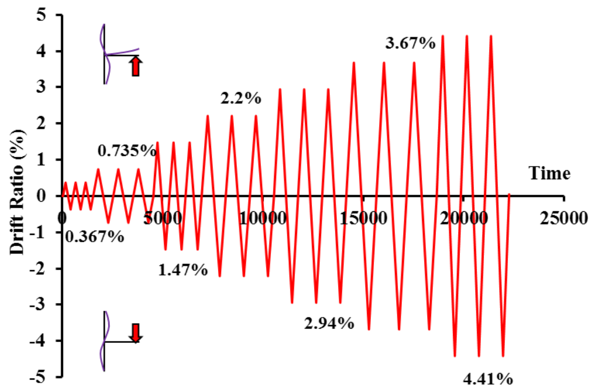

Fig. 6 Typical loading history used for the study

maximum displacements (Δl) applied are: ± 6.25 mm, ±12.5 mm, ±25.0 mm, ±37.5 mm, ±50 mm, ±62.5 mm and ±75 mm. First two drift increments ±6.25 mm, ±12.5 mm are elastic cycles. Yielding occurred at displacement of 25 mm. The further drift increments ±37.5 mm, ±50 mm, ±62.5 mm and ±75 mm are arrived by constantly increasing the displacement by ±12.5 mm from previous step and thereby resulting in more inelastic excursions. Three cycles are applied at each drift ratio. The drift ratio is specified as given in Eq. (1).

$$\text{Drift ratio (\%)} = (\Delta l / l_b) \times 100 \qquad (1)$$

Where, Δl=the applied displacement at the beam tip; and l_b=distance from column face to the point of application of the displacement. All the five GLD specimens i.e., one uncorroded control specimen (SP1), two corroded specimens (SP1-C1 and SP1-C2) and one each of strengthened uncorroded (SP1-R1) and corroded specimens (SP1-C3-R1) using steel bracket and haunch system are tested by subjecting them to the loading history shown in Fig. 6. Positive drift produces tension at beam bottom and negative drift produces tension at beam top. Load displacement hystereses and other data are acquired for all the five specimens and the data are processed. The comparative performance of the corroded specimens with that of the uncorroded control specimens is evaluated.

6. Estimation of level of corrosion in the beam reinforcements of corroded specimens SP1-C1, SP1-C2 and SP1-C3-R1

Upon completion of reverse cyclic tests, the beam reinforcement bars from the beam-column sub-assemblages SP1-C1, SP1-C2 and SP1-C3-R1 are extricated by removing the surrounding concrete as shown in the Fig. 7. It is also witnessed that the column main reinforcement bars and stirrups are uncorroded, in view of the insulation provided. The locations of the beam reinforcements in the beam-column sub-assemblage and their designations are shown in Fig. 8. The extricated reinforcement bars are cleaned with acid solution prepared as prescribed in ASTM G1-03 (2011). The percentage mass loss due to corrosion is estimated by gravimetric method as given below

Fig. 7 Extrication of beam reinforcement bars from corroded GLD specimens

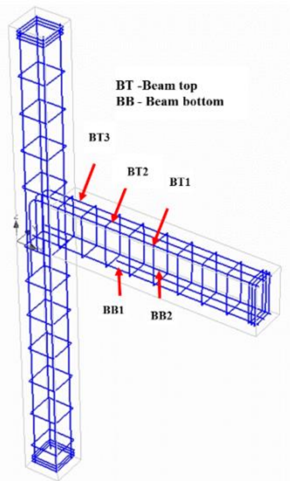

Fig. 8 Designation of beam reinforcement bars in GLD specimens

$$\text{Mass loss (\%)} = \frac{\mathrm{w}_{bc} - \mathrm{w}_{\mathrm{ac}}}{\mathrm{w}_{bc}} \mathrm{x}100 \tag{2}$$

Where, w_{bc} is the mass of uncorroded rebar and w_{ac} is the mass of corroded rebar after acid cleaning. By weighing the uncorroded segment of the rebar of known length, the mass per unit length of the uncorroded rebar is calculated and is used for calculating initial mass before corrosion of rebar segments of definite length collected from the corroded part of the beam main reinforcement. The mass of corroded rebar segment after acid cleaning is evaluated by weighing the corroded rebar segment using weighing balance. The average level of corrosion of beam reinforcement at a particular location of the beam from the joint region is evaluated by weighted average of corrosion levels of rebars in proportion to the area of reinforcement with respect to total area of steel.

For example, as the beam top has 2 numbers of 20 mm diameter bars and 1 number of 16mm diameter bar, the average level of corrosion at beam top is estimated as given below

$$\begin{aligned}&\text{Average level of corrosion (\%)}\\&= \frac{\boldsymbol{A_{20}W_{1,20}}}{\boldsymbol{A_t}} + \frac{\boldsymbol{A_{16}W_{16}}}{\boldsymbol{A_t}} + \frac{\boldsymbol{A_{20}W_{2,20}}}{\boldsymbol{A_t}}\end{aligned} \tag{3}$$

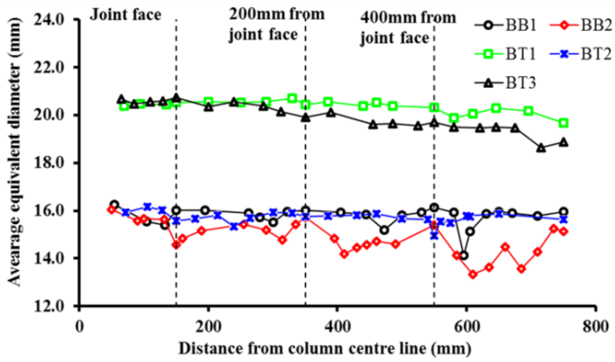

Fig. 9(a) Diameter profile of corroded beam main reinforcement bars of specimen SP1-C1

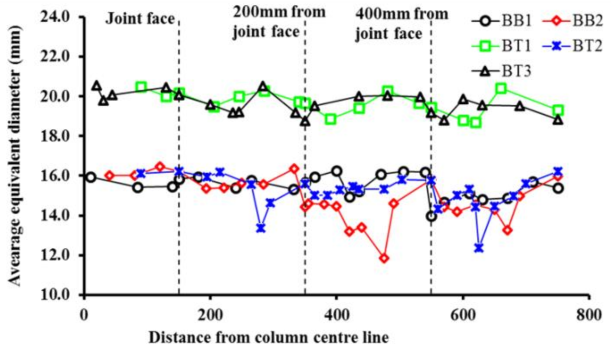

Fig. 9(b) Diameter profile of corroded beam main reinforcement bars of specimen SP1-C2

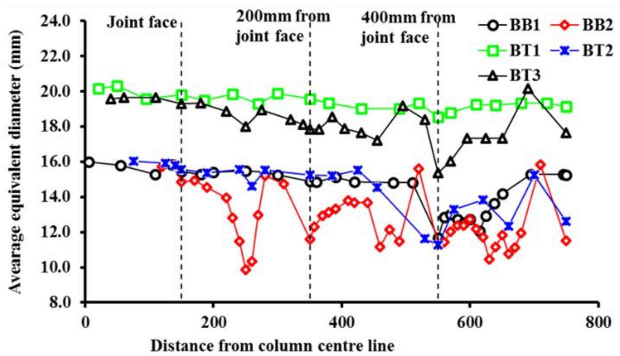

Fig. 9(c) Diameter profile of corroded beam main reinforcement bars of specimen SP1-C3-R1

Where, A_{20}, A_{16}, A_t are the areas of 20 mm diameter bar, 16 mm diameter bar and total steel respectively. $W_{1,20}$, W_{16} and $W_{2,20}$ are the percentage mass loss of first 20 mm bar, 16 mm bar and second 20 mm diameter bar respectively. The percentage mass loss due to corrosion is evaluated for all the reinforcement bars at beam top and bottom for the corroded specimens SP1-C1, SP1-C2 and SP1-C3-R1. Based on the above procedure, average levels of corrosion of beam top and bottom reinforcements are also calculated. The average mass loss of beam top and bottom reinforcements of specimens are presented in Table 3. Furthermore, the diameter profiling of the rebars along the length of the reinforcement bars is also carried out and is shown in Fig. 9. The equivalent diameter of reinforcement bar at any given location along the length of the beam main rebar is arrived by measuring the diameter using Vernier caliper at four different points around the circumference of the bar at that location. Based on the equivalent diameter profiling of the rebars, the nature of corrosion observed in rebars is grouped into three categories as (i) uniform corrosion (ii) non-uniform corrosion (iii) formation of localised pits.

It could be observed from Fig. 9(a) that the corrosion of rebar BB1 in specimen SP1-C1 is nearly uniform. The rebar BB2 of specimen SP1-C1 showed non-uniform corrosion up to a distance of 400mm from the face of the joint and localised pit formation beyond 400mm from the face of the joint. It could also be observed that beam top rebars (BT1-BT3) of SP1-C1 showed almost uniform corrosion along the length of the bar (Fig. 9(a)). From Fig. 9(b), localised pit formation could be observed in SP1-C2 for rebars BB1 and BB2 between 200 to 400 mm from joint face and the reduction in effective diameter is huge in rebar BB2 when compared with rebar BB1. Localised pit formation is observed between joint face and 200 mm from joint face in rebar BT2 of SP1-C2. Non-uniform corrosion of beam top bars BT1 and BT3 is observed in the specimen SP1-C2.

From Fig. 9(c), the rebars BB1, BT2, BT3 of specimen SP1-C3-R1 showed localised pit formation beyond 400mm from face of the joint and showed nearly uniform corrosion till 400mm from face of the joint. The rebar BB2 showed severe pitting corrosion along the length of rebar (Fig. 9(c)). The rebar BT1 showed nearly uniform corrosion along the length of the bar. Thus, even in the controlled environment (i.e., under laboratory condition) it would be difficult to produce uniform corrosion in rebar as the level of corrosion is function of properties such as diffusion, resistance, cover thickness, etc. of heterogeneous concrete. Moreover, the rebars that will be degraded due to natural environmental corrosion would also exhibit all these categories. Thus, the observations from the study would be directly useful to predict the behaviour of sub-assemblages corroded due to natural process.

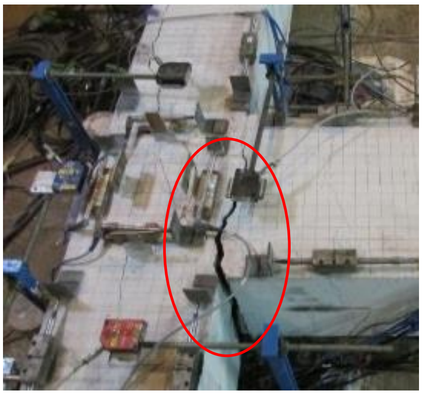

Damage at +50 mm (+2.94%)

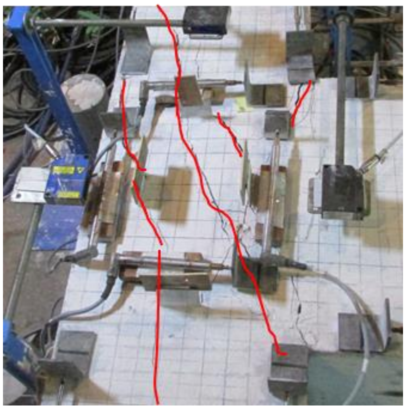

Damage at -50 mm (-2.94%)

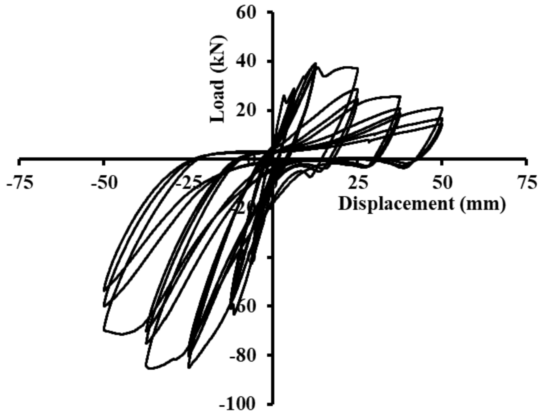

Fig. 10 Load-displacement hysteresis and damage at final drift cycles of uncorroded GLD specimen SP1

7. Results and discussions

7.1 Load-displacement hysteresis

7.1.1 Load-displacement behaviour of uncorroded GLD specimen SP1

The load-displacement hysteresis curves obtained for uncorroded GLD specimen SP1 are shown in Fig. 10. The maximum loads carried by the specimen in positive and negative cycles are 39 kN and 85 kN respectively. The huge difference in the maximum load carried in positive and negative drift cycles is due to unequal reinforcements at beam top and bottom in view of gravity load detailing. The uncorroded control GLD specimen showcased a poor hysteretic performance by encountering brittle mode of failure in both positive and negative cycles. During the positive cycle, at the displacement of 25 mm (drift ratio of 1.47%), the joint crack is opened-up due to anchorage failure of beam bottom bars. With further displacement increment, the damage progression has happened in the form of widening of the joint crack and resulted in huge reduction in load carrying capacity. At the displacement of 50 mm (drift ratio +2.94%), joint crack width of 13 mm is observed and the load is dropped to residual capacity of beam.

During negative cycle, at -25 mm (-1.47% drift ratio), fine joint shear cracks are appeared and yielding of beam top reinforcement bars is also observed. With further displacement increment, the widening of joint shear cracks is observed. This could be witnessed by strength degradation behaviour in the load-displacement curve at the displacement of -50 mm (-2.94% drift ratio). Thus, the uncorroded GLD specimen encountered anchorage failure and joint shear degradation in the positive and negative cycles of loading respectively and exhibited poor hysteretic performance.

Damage at +50 mm (+2.94%)

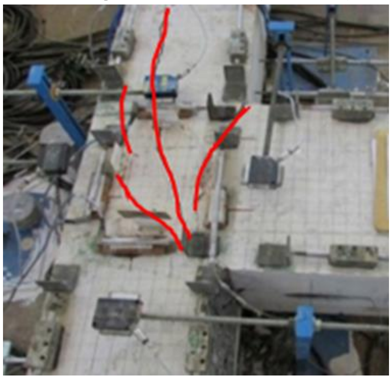

Damage at -50mm (-2.94%)

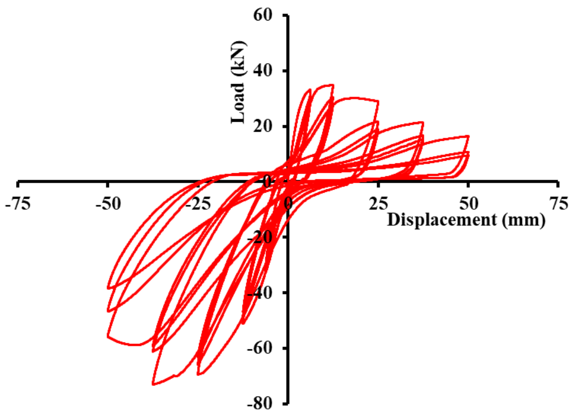

Fig. 11 Load-displacement hysteresis and damage at final drift cycles of corroded GLD specimen SP1-C1

7.1.2 Load-displacement behaviour of corroded GLD specimen SP1-C1

The load-displacement hysteresis curves obtained for corroded GLD specimen SP1-C1 along with damage patterns at final positive and negative drift cycles are shown in Fig. 11. The maximum load carried by SP1-C1 in positive and negative cycles are 35 kN and 73 kN respectively. The corroded specimen SP1-C1 showed similar load-displacement and damage progression behaviour as that of the uncorroded specimen SP1, i.e., it encountered anchorage failure by opening up of joint crack in positive cycle of loading and joint shear degradation in the negative cycle of loading. But the load carried by the specimen is lower when compared with the uncorroded specimen in both positive and negative cycles. The reduction in maximum loads in positive and negative cycles of corroded GLD specimen SP1-C1 are 11% and 15% respectively, compared with the corresponding maximum loads carried by uncorroded control GLD specimen SP1. The average levels of corrosion in beam bottom and top reinforcements of SP1-C1 are 14% and 6% respectively. Further, corroded specimen SP1-C1 showed wider cracks when compared with that of uncorroded specimen. This may be probably due to the weakening of concrete due to corrosion cracking. During the positive cycle of +37.5 mm (2.2% drift ratio), spalling of cover concrete from the inner face of column is also observed along with the widening of joint crack. Further, in the negative cycle, the joint shear cracks formed are wider when compared with that in uncorroded specimen SP1. It is essential to highlight the fact that all the rebars of SP1-C1 showed uniform corrosion except rebar BB2 which showed non-uniform corrosion. The poor hysteretic performance of GLD specimen is further aggravated by the corrosion of beam main reinforcement bars and is reflected in the form of lower load carrying capacity and more damage with wider cracks as witnessed in corroded GLD specimen SP1-C1.

7.1.3 Load-displacement behaviour of corroded GLD specimen SP1-C2

The load-displacement hysteresis curves obtained for corroded GLD specimen SP1-C2 along with damage progression at selected drift cycles are shown in Fig. 12. The load-displacement behaviour of the corroded specimen SP1-C2 is observed to be different compared with that of the uncorroded control GLD specimen SP1. The maximum loads carried by the corrosion damaged specimen SP1-C2 in the positive and negative cycles are 41 kN and 79 kN respectively. The average levels of corrosion in beam bottom and top reinforcements in SP1-C2 are 13.8% and 10.9% respectively. The slightly higher load carried by the corrosion damaged specimen SP1-C2 in positive drift cycle is attributed to the shift in the anchorage failure in beam bottom bars from displacement level of 25 mm (1.47%) to 37.5 mm (2.2%). In the case of SP1-C2, due to localised corrosion pit formation in beam bottom reinforcement at a location between 200 mm-400 mm from the joint face, the damage progression happened in the form of widening of two prominent flexural cracks till the drift ratio of 1.47% (Fig. 12). Localised corrosion pit formation might have reduced the bond strength drastically, which subsequently resulted in concrete cracking at the location of pits and hence the bond force demand at the face of the joint location is reduced. With subsequent increase in drift, the joint could not sustain the force demand and is opened up. Further, the corroded GLD specimen SP1-C2 showed in-cyclic strength degradation at 37.5 mm (+2.2% drift ratio), after opening-up of joint crack (Fig. 12). Under the action of dynamic loading (in the event of earthquake), this in-cyclic strength degradation would result in unstable system and hence it is highly undesirable. At drift ratio of +2.94% (50 mm), the specimen reached its residual carrying capacity. It could be observed that after the anchorage failure at +2.2%, load drop in SP1-C2 is huge when compared with that observed in uncorroded control GLD specimen SP1.

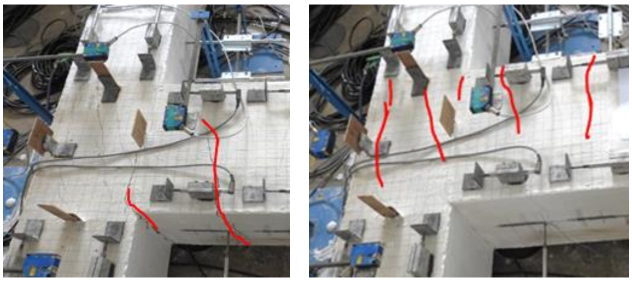

Damage at +25 mm (+1.47%) Damage at -12.5 (-0.735%)

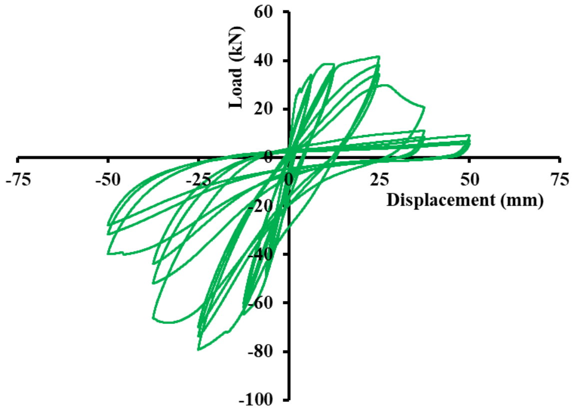

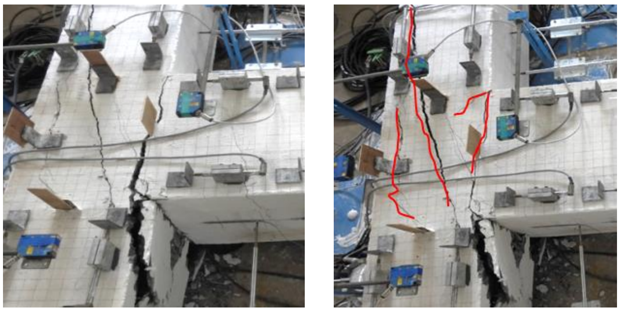

Damage at +50 mm (+2.94%) Damage at -50 mm (-2.94%)

Fig. 12 Load-displacement hysteresis and damage progression of corroded GLD specimen SP1-C2

Damage at +75 mm (+4.41%) Damage at -75 mm (-4.41%)

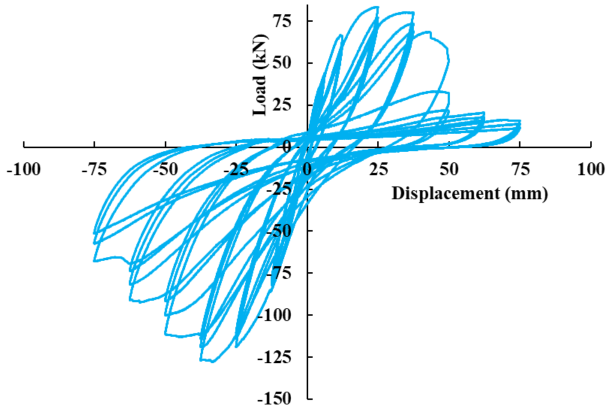

Fig. 13 Load-displacement hysteresis and damage at final drift cycles of uncorroded and strengthened GLD specimen SP1-R1

During the negative cycle, the specimen SP1-C2 showed damage progression in the form of two prominent flexural cracks at a distance between 200-400 mm from joint face and showcased better load-displacement behaviour till the displacement of -12.5 mm (-0.735%). At the drift ratio of -0.735%, diagonal shear cracking is also observed in the joint region. It could be observed that there is an advancement in the joint shear cracking in specimen SP1-C2 compared with the control specimen. After the drift ratio of -1.47%, the damage is manifested in the form of joint shear strength degradation. The specimen showed a strength degradation behaviour after displacement of 25mm (-1.47% drift ratio). As soon as the joint degradation began, the load carrying capacity of SP1-C2 is reduced more rapidly than that of the uncorroded specimen SP1 as can be seen from the load displacement hysteresis curves. Thus, the seismic performance is sensitive to the location and nature of corrosion in GLD beam-column sub-assemblages.

It could be observed that the average level of corrosion of beam bottom reinforcements is nearly same for both the corroded specimens SP1-C1 and SP1-C2. But the corroded specimens SP1-C1 and SP1-C2 showed different load displacement behaviour as it is dependent on the nature and the location of corrosion. Even though the average level of corrosion of beam top reinforcements of specimen SP1-C2 is higher than that of SP1-C1, SP1-C2 specimen carried higher load when compared with that of specimen SP1-C1 during negative cycle but the load drop after peak load is much larger in SP1-C2 when compared with SP1-C1. Thus, it could be inferred that corrosion of reinforcement is not only associated with reduction in load carrying capacity but also results in undesirable behaviour as observed in the case of corroded specimen SP1-C2. Hence, for GLD beam column sub-assemblages with deficiencies similar to that considered in the present study, it is difficult to establish the relation between the level of corrosion and the reduction in load carrying capacity of corroded specimen compared with that of uncorroded control specimen, as the behaviour of corroded specimen is sensitive to the location and nature of corrosion.

7.1.4 Load-displacement behaviour of externally strengthened uncorroded GLD specimen SP1-R1

The load-displacement hysteresis curves and damage progression at final drift cycles for uncorroded GLD specimen externally strengthened using steel bracket and haunch system (SP1-R1) are shown in Fig. 13. The maximum load carried by the strengthened specimen SP1-R1 in the positive and negative cycles of loading are 83 kN and 128 kN respectively. During the positive cycle, the anchorage failure of beam bottom bars is prevented at the displacement cycle of +25 mm (+1.47%) and yielding of beam reinforcement is observed at the same displacement

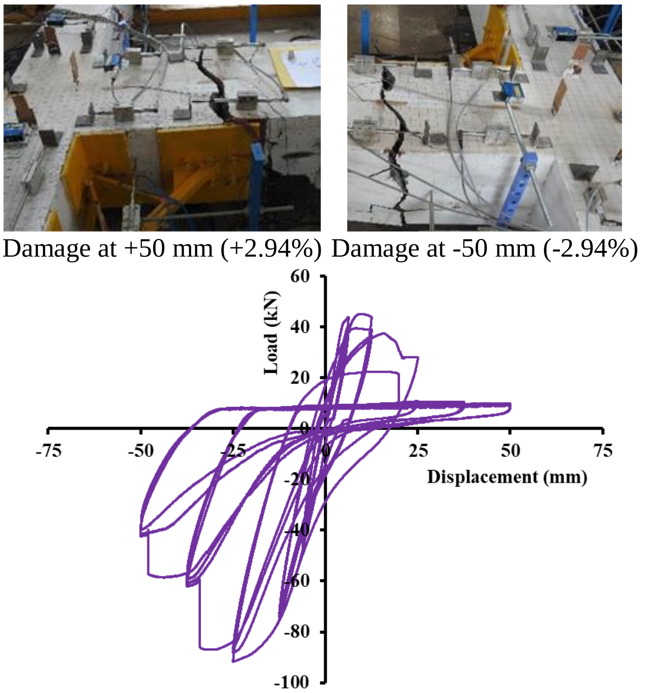

Fig. 14 Load-displacement hysteresis and damage at final drift cycles of strengthened corroded GLD specimen SP1-C3-R1

cycle. Further, opening up of joint at +25 mm cycle is not observed and damage progression had happened in the form of flexural cracking of beam at the haunch location. During the negative cycle of loading, the joint shear degradation is delayed to a large extent. The damage progression happened in the form of mixed mode i.e., the flexural cracking of beam and joint shear cracking. The peak load carried by the strengthened uncorroded GLD specimen SP1-R1 is much more than the peak load carried by the uncorroded GLD specimen SP1. These are the contrasting responses attained by externally strengthened uncorroded GLD specimen SP1-R1 by overcoming the major weaknesses of uncorroded GLD specimen SP1. This enhanced performance of externally strengthened uncorroded GLD specimen (SP1-R1) when compared with control uncorroded GLD specimen SP1 has prompted to adopt the same external strengthening scheme for improving the performance of corroded GLD specimen under reverse cyclic loading.

7.1.5 Load-displacement behaviour of externally strengthened corroded GLD specimen SP1-C3-R1

The load-displacement hysteresis curves and damage progression at final drift cycles for externally strengthened corroded GLD specimen (SP1-C3-R1) using steel bracket and haunch system are shown in Fig. 14. The externally strengthened corroded specimen SP1-C3-R1 showcased completely different load-displacement behaviour when compared with strengthened uncorroded GLD specimen SP1-R1. The maximum loads carried by specimen SP1-C3-R1 during positive and negative are 45 kN and 92 kN. In case of specimen SP1-C3-R1, during positive cycle of loading, till the displacement level of 25 mm (1.47% drift ratio), the damage progression happened in the form of widening of flexural crack located at about 400 mm from the face of the joint. Beam bottom bar BB2 showed severe pitting at a distance of 100 mm and 400 mm from the face of the joint. Both beam bottom bars showed localised pits at the distance of 400 mm from the joint and further the moment is maximum at this location due to haunch. Thus, the damage progression happened similar to corroded specimen SP1-C2. At the displacement of 25 mm, during first and second cycles of loading one of the beam bottom rebars got fractured and load is dropped to residual capacity in the third cycle of +25 mm. The specimen exhibited huge in-cyclic strength degradation at the drift ratio of +1.47% (25 mm). This is highly undesirable as it would result in unstable system under earthquake loading. Complete opening of beam at the haunch connection and spalling of cover concrete is witnessed at 50 mm displacement cycle (+2.94% drift cycle) (Fig. 14).

During negative cycle of loading, the damage progression has happened in the form of flexural cracking of beam at the location of haunch connection, as at this section beam top bars showed severe pitting and also happened to be the maximum moment location. Up to the displacement of -25 mm (-1.47% drift ratio), the damage progression has happened in the form of flexural cracking around 400mm from the face of the joint i.e. at the haunch connection. At the drift of -1.47%, horizontal cracks along the reinforcement bar are formed. At the displacement level of -37.5 mm (-2.2%), one of the beam top rebars got fractured and resulted in huge in-cyclic strength degradation. With further displacement increment to -50mm (-2.94%), the damage progression happened in the form of widening of horizontal crack (Fig. 14) and one more beam top bar got fractured which again resulted in huge in-cyclic strength degradation. In the case of specimen SP1-C3-R1, the location of localised pits and maximum load demand are happened to be at the same location and the corrosion of reinforcement resulted in brittle fracturing of rebars causing huge in-cyclic strength degradation in both positive and negative cycles of loading. This clearly brings out the immense seismic risk associated with corroded GLD beam column sub-assemblage. Further, this also put forwarded the fact that the strength of the corroded rebars cannot be relied upon while formulating seismic strengthening of corroded GLD beam-column sub-assemblage.

In the corroded specimens SP1-C2 and SP1-C3-R1, the damage progression happened at the location of localised corrosion pit formation on the rebar. When the locations of pits and maximum load demand coincide, as in the case of SP1-C3-R1, brittle fracture of reinforcement bar along with in-cyclic strength degradation has been witnessed. Further, the strengthened corroded specimen SP1-C3-R1 showcased under-performance when compared with that of strengthened uncorroded specimen SP1-R1, in terms of load carrying capacity as well as ductility. The maximum loads carried by the strengthened corroded GLD specimen SP1-C3-R1 are 46% and 28% lower than the maximum loads carried by the strengthened uncorroded GLD specimen SP1-R1 in positive and negative cycles of loading respectively. But, the load carried by the strengthened corroded GLD (SP1-C3-R1) specimen is nearly same as

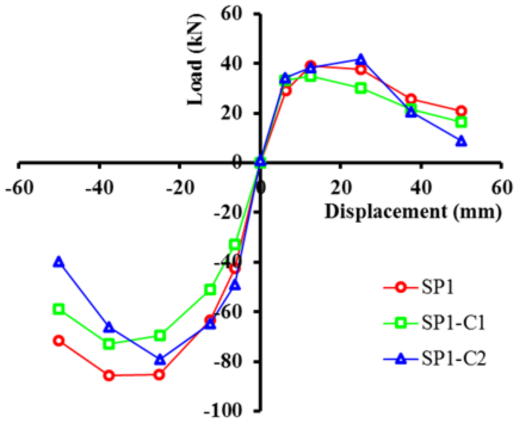

Fig. 15(a) Load-displacement envelopes of uncorroded and corroded GLD specimens

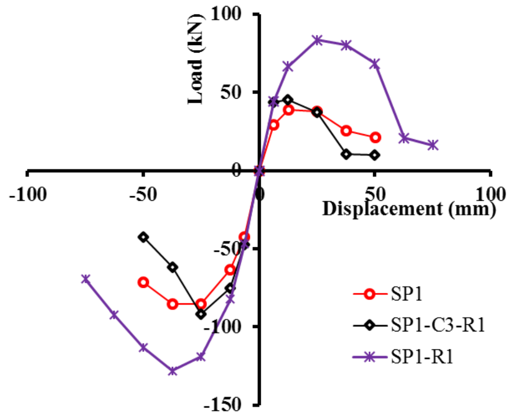

Fig. 15(b) Load-displacement envelopes of strengthened uncorroded and corroded GLD specimens

that of uncorroded GLD specimen SP1. However, SP1-C3-R1 showcased brittle fracture of rebars causing huge in-cyclic strength degradation. Thus, it could be concluded that the external strengthening which provides an alternate force flow path but relies on the strength of existing reinforcements is not able to mitigate the seismic risk of corroded members as the corroded reinforcement would encounter sudden fracture. Furthermore, it is very clear that it is not advisable to rely upon the strength of corroded rebar for mobilising the strength.

7.2 Load-displacement envelopes of specimens

The load-displacement envelopes for SP1, SP1-C1 and SP1-C2 are shown in Fig. 15(a). For specimens SP1 and SP1-C1, the load begins to drop after the displacement level of 12.5 mm (0.735% drift ratio). Whereas in the case of specimen SP1-C2, the load drop begins at drift ratio of +1.47% (25 mm displacement). Even though, corrosion damaged specimen SP1-C2 carried slightly higher load at +25 mm (1.47% drift ratio) displacement level when compared with that of SP1, the load carried at +50 mm (2.94%) displacement level is lower than that of both control (SP1) and another corrosion damaged specimen SP1-C1. The localised corrosion pit formation in SP1-C2, shifted the anchorage failure to higher drift ratio, but the residual capacity is reduced drastically and found to be lower than that of the uncorroded specimen in positive cycle of loading.

During the negative cycles, corrosion damaged specimen SP1-C1 carried lower load than the uncorroded control GLD specimen SP1 in all the cycles. The specimen SP1-C2 carried nearly same load as that of SP1 till the displacement cycle of -12.5 mm (-0.735% drift). The maximum load carried by both corroded specimens SP1-C1 and SP1-C2 are lower than the maximum load carried by the control specimen SP1. Further, it is observed that the load carried by the corrosion damaged specimen SP1-C2 is lower than that of the another corroded specimen SP1-C1 and uncorroded specimen SP1 at displacement levels of -37.5 mm (-2.2%) and -50 mm (-2.94%).

The load displacement envelopes of strengthened uncorroded GLD (SP1-R1) and corroded (SP1-C3-R1) GLD specimens are shown in Fig. 15(b). The externally strengthened corroded GLD specimen SP1-C3-R1 showed poor load carrying capacity at all drift cycles when compared with externally strengthened uncorroded GLD specimen SP1-R1. Further, for portraying the effect of strengthening on uncorroded and corroded GLD specimens, the load envelope of control uncorroded GLD specimen (SP1) without external strengthening is also shown in Fig. 15(b). The strengthened uncorroded specimen SP1-R1 showed enhanced load carrying capacity at all the drift ratios when compared with uncorroded GLD specimen SP1. This demonstrates the superior performance of externally strengthened uncorroded GLD specimen. The behaviour of SP1-C3-R1 is similar to that of specimen SP1 till drift ratio of +0.735% (12.5 mm) with slightly higher load carrying capacity when compared with that of SP1. At drift ratio of +1.47%, the specimen SP1-C3-R1 encountered fracturing of both beam bottom rebars, resulting in drastic reduction in the load carrying capacity when compared with that of SP1.

During negative cycles of loading, the behaviour of SP1-C3-R1 is similar to that of specimen SP1 till drift ratio of -1.47% (-25mm) with slightly higher load carrying capacity, and SP1-C3-R1 carried peak load at the drift ratio of -1.47%. Further, SP1-C3-R1 showed huge load drop after peak load. The strengthened corroded specimen SP1-C3-R1 could not catch up with that of strengthened uncorroded specimen SP1-R1. The improvement in load carrying capacity of strengthened corroded specimen is only up to the level of uncorroded specimen SP1. Beyond peak load, the performance of strengthened corroded specimen (SP1-C3-R1) is poor compared with that of SP1. Hence, it can be concluded that external strengthening which demonstrated exemplary performance in the case of uncorroded GLD specimen is found to be not that effective in enhancing the performance of corroded GLD specimen under reverse cyclic loading.

7.3 Nominal principal tensile stress in the joint

The nominal principal tensile stress is evaluated using Eq. (4) for uncorroded and corroded GLD specimens SP1, SP1-C1 and SP1-C2 and the variation of nominal principal tensile stress w.r.t drift ratio is presented in Fig. 16(a). During the positive cycle of loading, the nominal principal

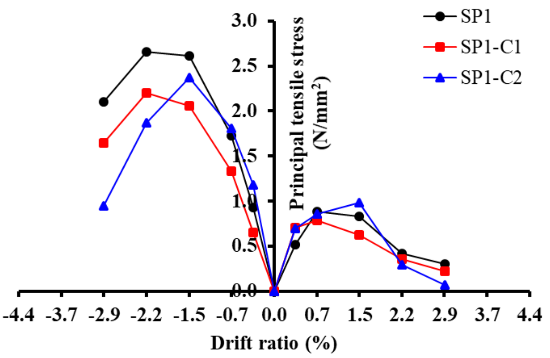

Fig. 16(a) Nominal principal tensile stress of uncorroded and corroded GLD specimens

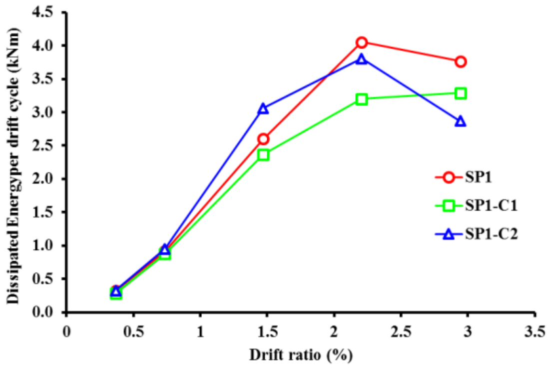

Fig. 17(a) Energy dissipation of uncorroded and corroded GLD specimens

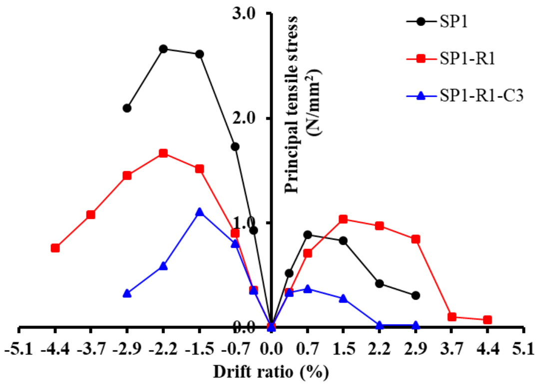

Fig. 16(b) Nominal principal tensile stress of strengthened uncorroded and corroded GLD specimens

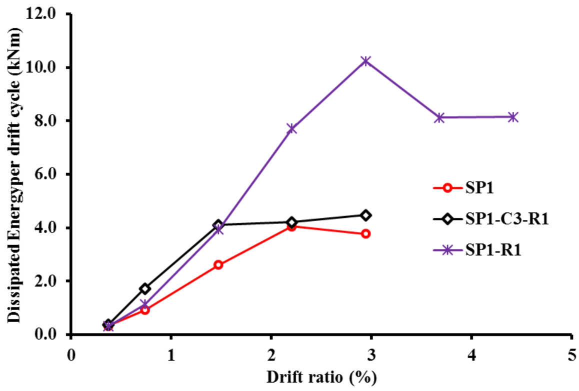

Fig. 17(b) Energy dissipation of strengthened uncorroded and corroded GLD specimens

tensile stress is well below the first cracking stress of 1.58 N/mm^2 ($0.29\sqrt{fc}$ as given by Priestly *et al.* (1997)). Hence, no cracking is witnessed in the sub-assemblage during positive cycle of loading. During the negative cycle of loading, both corroded as well as uncorroded GLD specimens encountered joint shear degradation. The joint degradation of the corroded specimens happened even though the principal tensile stress is less than that in uncorroded GLD specimen SP1. The nominal principal tensile stress of strengthened uncorroded and corroded GLD specimens is evaluated using Eq. (4) but the joint shear stress is evaluated corresponding to the reduced beam moment at joint face due to haunch retrofit. The details for evaluation of reduced beam moment at the joint face due to haunch retrofit can be found elsewhere (Kanchanadevi and Ramanjaneyulu 2018a). The variation of nominal principal tensile stress of strengthened uncorroded and corroded GLD specimens is shown in Fig. 16(b). From Fig. 16(b), it could be observed that nominal principal tensile stress is well below the first cracking stress for strengthened uncorroded specimen SP1-R1. In the case of strengthened corroded specimen SP1-R1-C3, the drop in principal stress is attributed to the reduction in V_j as the moment capacity of corroded specimen is less due to fracturing of rebar at the drift ratio of -2.22%.

$$p_t = -\frac{f_a}{2} + \sqrt{\left(\frac{f_a}{2}\right)^2 + v_{js}^2} \qquad (4)$$

$$v_{js} = V_j / A_e \qquad (5)$$

Where, V_j - horizontal joint shear force, v_{js} - Average shear stress in the joint, A_e - Effective area of joint defined in ACI 318(2011). p_t - nominal principal tensile stress of the joint. f_a - axial stress in the joint.

7.4 Energy dissipation

Energy dissipated by uncorroded and corroded GLD specimens SP1, SP1-C1 and SP1-C2 is presented in Fig. 17(a). It could be observed that the energy dissipated in each drift cycle for corroded (SP1-C1 and SP1-C2) and uncorroded (SP1) specimens are nearly same till the drift ratio of 0.735%. At the drift ratio of 1.47%, the energy dissipated by SP1-C2 is higher than GLD uncorroded specimen SP1 due to shifting of anchorage failure in view of localised corrosion pit formation in SP1-C2. But the corroded GLD specimen SP1-C1, showed slightly lower energy dissipation at 1.47% cycle when compared with SP1. After that both corroded specimens (SP1-C1 and SP1-C2) showed lower energy dissipation when compared with the uncorroded specimen SP1. Even though the load drop is huge in the case of corroded specimens, there is not much drop in the energy dissipation. This is due to the fact that the corroded specimens have undergone huge slip and lesser pinching when compared with that of the control uncorroded specimen and also formed wider hysteretic loop. At the drift ratio of 2.94%, the energy dissipated by the specimens SP1, SP1-C1 and SP1-C2 are found to be 3.77 kNm, 3.2 kNm and 2.87 kNm respectively.

The energy dissipated by externally strengthened uncorroded (SP1-R1) and corroded (SP1-C3-R1) GLD specimens are shown in Fig. 17(b). The specimen SP1-C3-R1 showed very much lower energy dissipation when compared with that of the specimen SP1-R1, due to fracturing of rebars at the location of corrosion pits causing in-cyclic strength degradation in the case of SP1-C3-R1. Further, the energy dissipated by uncorroded GLD specimen SP1 which is not externally strengthened is also shown in Fig. 17(b). A tremendous improvement in energy dissipation is observed in strengthened uncorroded specimen SP1-R1 when compared with that of SP1 in all the drift cycles. The externally strengthened corroded specimen SP1-C3-R1 showed little higher energy dissipation when compared with that of SP1. At the drift ratio of 2.94%, the energy dissipated by SP1, SP1-C3-R1 and SP1-R1 is found to be 3.76 kNm, 4.47 kNm and 10.23 kNm respectively. This little higher energy dissipation of SP1-C3-R1 over that of SP1 is attributed to the huge slip undergone by the specimen SP1-C3-R1, even though it carried the same load as that of the uncorroded specimen SP1. Thus, it may be concluded that the external strengthening which provided an alternate load path but depends on the strength of existing reinforcement, could not improve the energy dissipation capacity of corroded specimen, as it encountered brittle fracture of corroded rebars.

The energy dissipation capacity of corroded and uncorroded specimens are also expressed in terms of equivalent viscous damping co-efficient. The equivalent viscous damping co-efficient (Δ) is expressed by Eq. (6)

$$\Delta = \frac{1}{2\pi}\frac{Area\text{ enclosed by }hystersis\ loop}{Elastic\ strain\ energy} \tag{6}$$

The energy dissipation capacity of corroded and uncorroded specimens in terms of equivalent viscous damping co-efficient as shown in Fig. 18(a). It could be observed that initially at 0.37% drift ratio, the equivalent damping coefficients of the corroded specimens are small compared with that of uncorroded control specimen SP1. But with the increase in drift ratio, the damping coefficients evaluated for corroded specimens are higher than that of uncorroded control specimen SP1. This is more predominant in the case of SP1-C2 at drift ratio of 2.21% and 2.94%. This increased damping coefficient may be due to wider cracking of corroded specimens and increased area of hysteresis loop which is almost same as that of the uncorroded specimen; but the residual load carried by the corroded specimen is lower than that of the uncorroded specimen thus resulting in higher damping co-efficient. This higher damping coefficient evaluated using the above procedure presents a pseudo phenomenon. The equivalent viscous damping coefficients for strengthened uncorroded and corroded specimens are shown in Fig. 18(b). The damping co-efficient for specimen SP1-R1-C3 is higher than SP-R1 for all the drift ratios. In the case of specimen SP1-R1-C3, due to brittle fracturing of rebars, the specimen encountered in-cyclic strength degradation and low residual strength, thereby resulting in lower elastic strain energy and higher damping co-efficient, which is again a pseudo phenomenon.

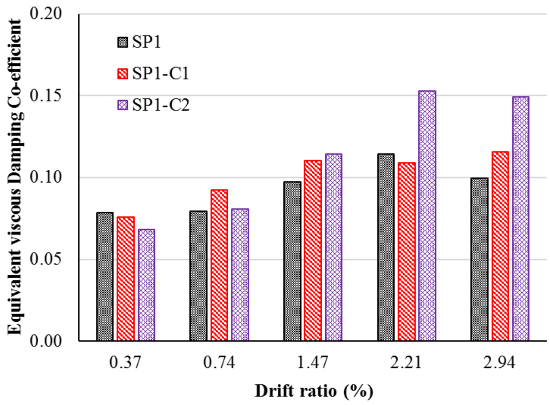

Fig. 18(a) Equivalent damping co-efficient of uncorroded and corroded GLD specimens

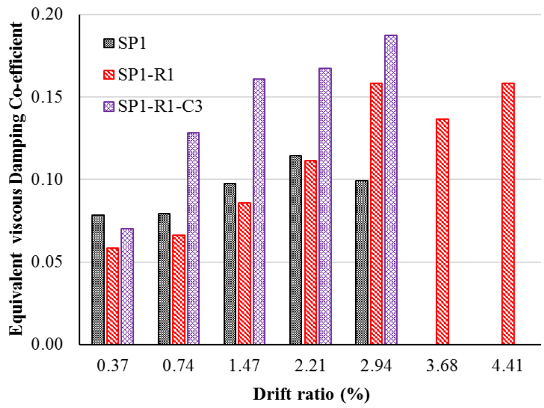

Fig. 18(b) Equivalent damping co-efficient of strengthened uncorroded and corroded GLD specimens

7.5 Damage index

The damage indices of the specimens are evaluated using damage model proposed by Park and Ang (1985) given by

$$D = \frac{\delta_m}{\delta_u} + \frac{\beta}{Q_y \delta_u}\int dE \tag{7}$$

where δ_m is the maximum deformation under seismic loading; δ_u is the ultimate deformation under monotonic load; Q_y is the calculated yield strength (If maximum strength is less than yield strength this has to be replaced by the maximum strength); dE is the incremental adsorbed hysteretic energy; β is the model parameter which represents the effect of cyclic loading on structural damage and depends on confinement ratio, shear span, longitudinal steel and axial stress level. In the present study, for the evaluation of damage index, the model parameter β is taken as 0.05 (Park *et al*. 1987). The damage indices obtained for uncorroded and corroded GLD specimens SP1, SP1-C1 and SP1-C2 are presented in Fig. 19(a). It could be observed that the damage indices of the corroded specimens are more than that of uncorroded GLD Specimen SP1 in all the drift cycles. The damage indices of externally strengthened

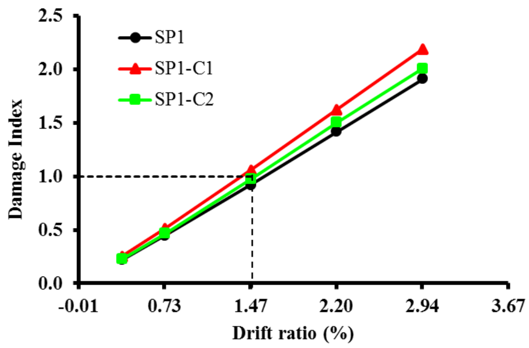

Fig. 19(a) Damage index of uncorroded and corroded GLD specimens

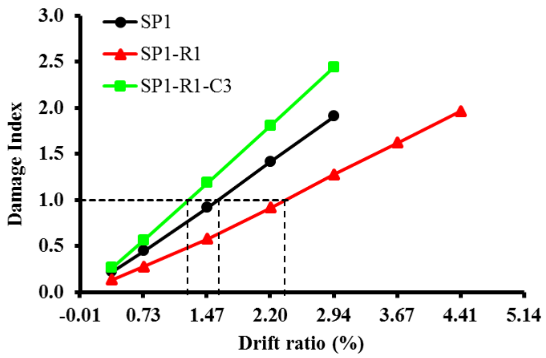

Fig. 19(b) Damage index of strengthened uncorroded and corroded GLD specimens

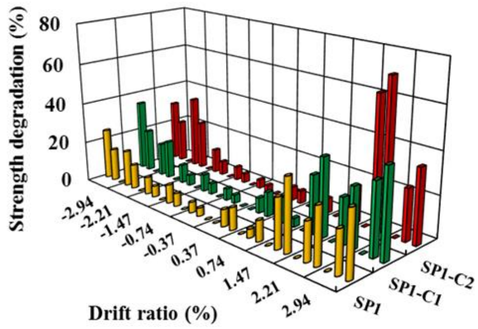

Fig. 20(a) Strength degradation of uncorroded and corroded GLD specimens

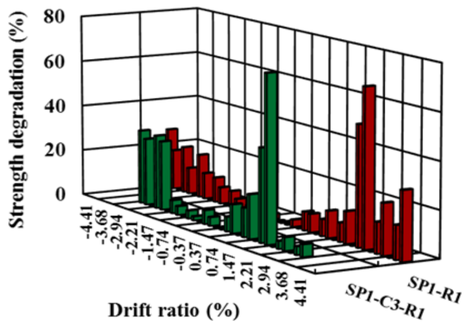

Fig. 20(b) Strength degradation of strengthened uncorroded and corroded GLD specimens

uncorroded (SP1-R1) and corroded (SP1-C3-R1) GLD specimens are shown in Fig. 19(b). It could be observed that the strengthened corroded specimen SP1-C3-R1 showed much higher damage index when compared with uncorroded GLD Specimen SP1. This may be due to formation of wider cracking and brittle fracturing of rebars. On the other hand, the damage index of strengthened uncorroded specimen SP1-R1 is much lower when compared with that of control GLD specimen SP1. This demonstrates the efficacy of the retrofit in mitigating the damage of uncorroded specimen. But the haunch retrofit is not up to the mark in mitigating the seismic risk associated with corroded GLD specimen.

7.6 Strength degradation

The strength degradation during the second and third cycles with respect to the maximum load of first cycle of each drift ratio is evaluated for the uncorroded (SP1) and corroded (SP1-C1 and SP1-C2) GLD specimens and is shown in Fig. 20(a). The strength degradation between the cycles is found to be less till the drift ratio of 0.735% in both positive and negative cycles for the specimens SP1, SP1-C1 and SP1-C2. Further, it is noted that the strength degradation between the first cycle and second cycle is more when compared with strength degradation between second and third cycles. The strength degradation of the specimens is found to be more in positive cycles when compared with that in negative cycles. The corroded specimens showed more strength degradation compared with uncorroded control specimen SP1. The maximum strength degradation incurred by specimens SP1, SP1-C1 and SP1-C2 in the positive cycle is found to be 34%, 42% and 71% respectively. During the negative cycles the maximum strength degradation incurred by specimens SP1, SP1-C1 and SP1-C2 is found to be 25%, 35% and 36% respectively. During negative cycle, both SP1-C1 and SP1-C2 specimens showed nearly same strength degradation but higher than that of uncorroded GLD specimen SP1.

The strength degradation of externally strengthened uncorroded (SP1-R1) and corroded (SP1-C3-R1) GLD specimens is shown in Fig. 20(b). The specimen SP1-C3-R1 showed more strength degradation than that of SP1-R1 at the drift ratio of +1.47%, due to fracturing of rebar. The specimen SP1-R1 showed maximum strength degradation at the drift ratio of +2.94% whereas the specimen SP1-C3-R1 showed maximum strength degradation at the drift ratio of +1.47%. The specimen SP1-C3-R1 showed more strength degradation when compared with SP1-R1 during the negative cycle of loading. The maximum strength degradation undergone by specimen SP1-C3-R1 during negative cycle of loading is more than that of SP1-R1.

8. Conclusions

Experimental investigations are carried out on GLD specimens, comprising of i) One uncorroded ii) Two corroded iii) One uncorroded strengthened with steel bracket and haunch iv) One corroded strengthened with steel bracket and haunch, under reverse cyclic loading. The conclusions drawn from the experimental investigations are as follows:

• In corroded GLD specimen SP1-C1, uniform corrosion is observed in all the rebars except rebar BB2 which showed non-uniform corrosion. SP1-C1 exhibited similar damage progression as well as load-displacement behavior as that of the control uncorroded specimen SP1. The poor hysteretic performance of GLD specimen under reverse cyclic loading is further degraded due to corrosion and reflected in terms of lower load carrying capacity and encountering more damage with wider cracks.

• Corroded GLD specimen SP1-C2 showcased different load-displacement as well as damage progression behaviour compared with that of the control uncorroded GLD specimen SP1. During positive cycle of loading, due to localized corrosion pit formations in the beam reinforcement, anchorage failure of beam bottom bars is delayed and shifted from +1.47% to +2.2% drift ratio but incurred a huge in-cyclic strength degradation at the drift ratio of +2.2%, which is undesirable from seismic view point.

• In the case of strengthened corroded GLD specimen SP1-C3-R1, the locations of localised pits and maximum load demand coincided and resulted in brittle fracturing of rebars causing huge in-cyclic strength degradation in both positive and negative cycles. The specimen SP1-C3-R1 showed a poor performance when compared with strengthened uncorroded specimen SP1-R1, in terms of load carrying capacity as well as ductility. The load carrying capacity of strengthened corroded specimen SP1-C3-R1 could reach only nearer to that of the uncorroded GLD specimen SP1, but far below that of SP1-R1. Furthermore, it is also very clear that it is not advisable to rely upon the strength of corroded rebar while formulating the seismic retrofit of corroded GLD beam-column sub-assemblages.

• From the study, it could be observed that uniform corrosion of reinforcement resulted in the behavior similar to that of uncorroded specimen with reduction in load carrying capacity and formation of wider cracks. In corroded specimens with localized corrosion pit formations, the damage progression is initiated at the location of corrosion pits and resulted in huge in-cyclic strength degradation. Furthermore, it is clear that it is not possible to establish the relation between the level of corrosion and the reduction in load carrying capacity of corroded specimen compared with that of control uncorroded specimen as the behaviour of corroded specimen is sensitive to the location and nature of corrosion.

• At the drift ratio of 2.94%, the energy dissipated by the specimens SP1, SP1-C1 and SP1-C2 are found to be 3.77 kNm, 3.2 kNm and 2.87 kNm respectively. Even though corroded specimens SP1-C1 and SP1-C2 showed huge drop in load after peak load when compared with SP1, there is not much drop in the energy dissipation. This is due to the fact that the corroded specimens have undergone huge slip and lesser pinching when compared with that of the control uncorroded specimen and also formed wider hysteretic loop.

• A tremendous improvement in energy dissipation is observed in the strengthened uncorroded specimen SP1-R1 when compared with that of uncorroded specimen SP1. Whereas the strengthened corroded specimen SP1-C3-R1 showed little higher energy dissipation when compared with that of SP1. At the drift ratio of 2.94%, the energy dissipated by SP1, SP1-C3-R1 and SP1-R1 is found to be 3.76kNm, 4.47 kNm and 10.23 kNm respectively.

• From the damage indices evaluated for uncorroded and corroded GLD specimens, it is observed that the damage indices of the corroded specimens are more than that of uncorroded GLD specimen in all the drift cycles. This may be due to formation of wider cracking and brittle fracturing of rebars.

• Corroded GLD specimens SP1-C1 and SP1-C2 showed more strength degradation when compared with that of uncorroded GLD specimen SP1 in both positive and negative cycles. The maximum strength degradation incurred by specimens SP1, SP1-C1 and SP1-C2 in the positive cycle is found to be 34%, 42% and 71% respectively. Similarly, during the negative cycles, the maximum strength degradation incurred by specimens SP1, SP1-C1 and SP1-C2 is found to be 25%, 35% and 36% respectively. The strengthened corroded specimen SP1-C3-R1 showed more strength degradation when compared with strengthened uncorroded specimen SP1-R1.

Thus, present study brings out the fact that the behaviour of corrosion affected beam-column sub-assemblages subjected to reverse cyclic loading is highly dependent on location and nature of corrosion. The immense seismic risk associated with the corrosion affected GLD beam-column sub-assemblages is also highlighted. Furthermore, the study also gives a clear suggestion not to utilise the strength of existing reinforcements while formulating strategies for seismic strengthening of corrosion affected GLD beam column sub-assemblage.

Acknowledgments

The authors wish to express their heartfelt thanks to staff members of Advanced Concrete Testing & Evaluation Laboratory and Structural Testing Laboratory for their cooperation during the experimental investigations.

References

ACI 318M-11, Building Code Requirements for Structural Concrete and Commentary.

ASTMG1-03 (2011), Standard Practice for Preparing, Cleaning, and Evaluating Corrosion Test Specimens.

Bhargava, K., Ghosh, A.K., Mori, Y. and Ramanujam, S. (2007), "Models for corrosion-induced bond strength degradation in reinforced concrete", *ACI Mater. J.*, **104**, 594-603.

Calvi, G.M., Magenes, G. and Pampanin, S. (2001), "Experimental test on a three storey RC frame designed for gravity only", *12th European Conference on Earthquake Engineering*, London, Paper Reference 727.

Campione, G., Cavaleri, L. and Papia, M. (2015), "Flexural response of external R.C. beam-column joints externally strengthened with steel cages", *Eng. Struct.*, **104,** 51-64.

Cardone, D., Perrone, G. and Sofia, S. (2013), "Experimental and numerical studies on the cyclic behavior of R/C hollow bridge piers with corroded rebars", *Earthq. Struct.*, **4**(1), 41-62.

Chung, L., Kim, J.H.J. and Yi, S.T. (2008), "Bond strength prediction for reinforced concrete members with highly corroded reinforcing bars", *Cement Concrete Compos.*, **30**, 603-611.

Dhakal, R.P., Pan, T.C., Irawan, P., Tsai, K.C., Lin, K.C. and Chen, C.H. (2005), "Experimental study on the dynamic response of gravity-designed reinforced concrete connections", *Eng. Struct.*, **27**(1), 75-87.

El-Attar, A.G., White, R.N. and Gergely, P. (1997), "Behaviour of gravity load designed reinforced concrete buildings subjected to earthquakes", *ACI Struct. J.*, **94**(2), 133-145.

Fang, C., Lundgren, K., Plos, M. and Gylltoft, K. (2006), "Bond behaviour of corroded reinforcing steel bars in concrete", *Cement Concrete Res.*, **36**, 1931-1938.

Goksu, C. and Ilki, A. (2016), "Seismic behavior of reinforced concrete columns with corroded deformed reinforcing bars", *ACI Struct. J.*, **113**(5), 1053-1064.

Guan, Y. and Zheng, S. (2018), "Seismic behaviors of RC frame beam-column joints under acid rain circle: A pilot experimental study", *J. Earthq. Eng.*, **22**(6), 1008-1026.

Hadigheh, S.A., Mahini, S.S. and Maheri, M.R. (2014), "Seismic behavior of FRP-retrofitted reinforced concrete frames", *J. Earthq. Eng.*, **18**, 1171-1197.

Humar, J.M., Lau, D. and Pierre, J.R. (2001), "Performance of buildings during the 2001 Bhuj earthquake", *Can. J. Civil Eng.*, **28**, 979-991.

Imperatore, S., Rinaldi, Z. and Drago, C. (2017), "Degradation relationships for the mechanical properties of corroded steel rebars", *Constr. Build. Mater.*, **148**, 219-230.

Jain, S.K., Murty, C.V.R. and Chandak, N. (1994), "The September 29, 1993, M6.4 Killari, Maharashtra Earthquake in Central India", EERI Special Earthquake Report, EERI Newsletter, **28**(1), January.

Kakaletsis, D.J., David, K.N. and Karayannis, C.G. (2011), "Effectiveness of some conventional seismic retrofitting techniques for bare and infilled R/C frames", *J. Struct. Eng. Mech.*, **39**(4), 499-520.

Kalogeropoulos, G.I., Tsonos, A.G., Konstandinidis, D. and Tsetines, S. (2016), "Pre-earthquake and post-earthquake retrofitting of poorly detailed exterior RC beam-to-column joints", *Eng. Struct.*, **109**, 1-15.

Kanchanadevi, A. and Ramanjaneyulu, K. (2017), "Comparative performance of seismically deficient exterior beam-column sub-assemblages of different design evolutions: A closer perspective", *Earthq. Struct.*, **13**(2), 177-191.

Kanchanadevi, A. and Ramanjaneyulu, K. (2018a), "Non-invasive steel haunch upgradation strategy for seismically deficient reinforced concrete exterior beam-column sub-assemblages", *Steel Compos. Struct.*, **28**(6), 719-734.

Kanchanadevi, A. and Ramanjaneyulu, K. (2018b), "Effect of corrosion damage on seismic behaviour of existing reinforced concrete beam-column sub-assemblages", *Eng. Struct.*, **174**, 601-617

Kanchanadevi, A., Ramanjaneyulu K., Mayank, T. and Saptarshi S. (2018), "Novel non-invasive seismic upgradation strategies for gravity load designed exterior beam-column joints", *Arch. Civil Mech. Eng.*, **18**, 479- 489.

Kheyroddin, A., Khalili, A., Emami, E. and Sharbatdar, M.K. (2016), "An innovative experimental method to upgrade performance of external weak RC joints using fused steel prop plus sheets", *Steel Compos. Struct.*, **21**(2), 443-460.

Kunnath, S.K., Hoffmann, G., Reinhorn, A.M. and Mander, J.B. (1995), "Gravity load-designed reinforced concrete buildings-Part II: Evaluation of detailing enhancements", *ACI Struct. J.*, **92**(4), 470-478.

Lee, H.S., Noguchi, T. and Tomosawa, F. (2002), "Evaluation of the bond properties between concrete and reinforcement as a function of the degree of reinforcement corrosion", *Cement Concrete Res.*, **32**, 1313-1318.

Li, J., Gong, J. and Wang, J. (2009), "Seismic behavior of corrosion-damaged reinforced concrete columns strengthened using combined carbon fiber-reinforced polymer and steel jacket", *Constr. Build. Mater.*, **23**, 2653-2663.

Liu, X., Jiang, H. and He, L. (2017), "Experimental investigation on seismic performance of corroded reinforced concrete moment-resisting frames", *Eng. Struct.*, **153**, 639-652.

Melo, J., Varum, H. and Tiziana Rossetto, T. (2015), "Cyclic behaviour of interior beam-column joints reinforced with plain bars", *Earthq. Eng. Struct. Dyn.*, **44**, 1351-1371.

Natesan, M., Venkatachari, G. and Palaniswamy, N. (2005), "Corrosivity and durability maps of India", *Corr. Prevent. Control*, **52**(2), 43-55.

Ou, Y.C. and Nguyen, N.D. (2016), "Influences of location of reinforcement corrosion on seismic performance of corroded reinforced concrete beams", *Eng. Struct.*, **126**, 210-223.

Pampanin, S., Bolognini, D. and Pavese, A. (2007), "Performance-based seismic retrofit strategy for existing reinforced concrete frame system using fiber-reinforced polymer composites", *J. Compos. Constr.*, ASCE, **11**, 211-226.

Pantelides, C.P., Hansen, J., Nadauld, J. and Reaveley, L.D. (2002), "Assessment of Reinforced Concrete Building Exterior Joints with Substandard Details", PEER Report 18, University of California, Berkeley.

Park, Y. and Ang, A. (1985), "Mechanistic seismic damage model for reinforced-concrete", *J. Struct. Eng.*, ASCE, **111**(4), 722-739.

Park, Y.J., Ang, A.H.S. and Wen, Y.K. (1987), "Damage-limiting aseismic design of buildings", *Earthq. Spectra*, **3**(1), 1-26.

Priestley, M.J.N. (1997), "Displacement-based seismic assessment of reinforced concrete buildings", *J. Earthq. Eng.*, **1**(1), 157-192.

Realfonzo, R., Napoli, A. and Pinilla, J.G.R. (2014), "Cyclic behavior of RC beam-column joints strengthened with FRP systems", *Constr. Build. Mater.*, **54**, 282-297.

Santarsiero, G. and Masi, A. (2015), "Seismic performance of RC beam-column joints retrofitted with steel dissipation jackets", *Eng. Struct.*, **85**, 95-106.

Sezen, H. (2012), "Repair and strengthening of reinforced concrete beam-column joints with fiber-reinforced polymer composites", *J. Compos. Constr.*, **16**(5), 499-506.

Sharma, A., Reddy, G.R., Eligehausen, R., Genesio, G. and Pampanin, S. (2014), "Seismic response of reinforced concrete frames with haunch retrofit solution", *ACI Struct. J.*, **111**(3), 673-684.

Tsonos, A.G. (2008), "Effectiveness of CFRP-jackets and RC-jackets in post-earthquake and pre-earthquake retrofitting of beam-column sub-assemblages", *Eng. Struct.*, **30**, 777-793.

Tsonos, A.G. (2014), "An innovative solution for strengthening of old R/C structures and for improving the FRP strengthening method", *Struct. Monit. Mainten.*, **1**(3), 323-338.

Tsonos, A.G. and Papanikolaou K.V. (2003), "Post-earthquake repair and strengthening of RC beam-column connections (theoretical & experimental investigation)", *Bull. NZ Soc. Earthq. Eng.*, **36**(2), 73-79.

Wang, H. (2009), "An analytical study of bond strength associated with splitting of concrete cover", *Eng. Struct.*, **31**, 968-975.

Wu, Y.Z., Lv, H.L., Zhou, S.C. and Fang, Z.N. (2016), "Degradation model of bond performance between deteriorated concrete and corroded deformed steel bars", *Constr. Build.*

Mater., **119**, 89-95.
Yavari, S., Elwood, K.J., Wu, C.L., Lin, S.H., Hwang, S.J. and Moehle, J.P. (2013), "Shaking table tests on reinforced concrete frames without seismic detailing", *ACI Struct. J.*, **110**(6), 1001-1012.
Yüksel, I. (2015), "Rebar corrosion effects on structural behavior of buildings", *Struct. Eng. Mech.*, **54**(6), 1111-1133.
Zhou, H., Liang X., Wang, Z., Zhang, X. and Xing, F. (2017), "Bond deterioration of corroded steel in two different concrete mixes", *Struct. Eng. Mech.*, **63**(6), 725-734.
Zhu, W. and François, R. (2013), "Effect of corrosion pattern on the ductility of tensile reinforcement extracted from a 26-year-old corroded beam", *Adv. Concrete Constr.*, **1**(2), 121-136.

AT